science, engineering and health studies

Research Article

Science, Engineering and Health Studies
https://lio1.tci-thaijo.org/index.php/sehs
ISSN (Online): 2630-0087

Landslide susceptibility assessment in Sabah, Malaysia: A bivariate frequency ratio approach

Rodeano Roslee[1,2] and Rishanthiny Bala Krishnan[1,2]*

[1] Natural Disaster Research Centre (NDRC), Universiti Malaysia Sabah, Kota Kinabalu, Sabah 88400, Malaysia
[2] Faculty of Science & Natural Resources (FSSA), Universiti Malaysia Sabah, Kota Kinabalu, Sabah 88400, Malaysia

ABSTRACT

A statistical bivariate model, frequency ratio, was used to assess the susceptibility of Pekan Nabalu to Kundasang area to landslides, using a geographic information system as a tool because the number of reported landslide cases rises annually. A total of 564 landslides (0.27 km^2) were detected from field observations, Google Earth satellite imagery, and IFSAR imagery, creating a landslide inventory map (dependent factor). To determine landslide susceptibility, eight landslide causative factor maps (independent factor) were considered: slope angle, slope aspect, slope curvature, drainage proximity, lineament proximity, lithology, land use, and soil series. The integration of these dependent and independent factors resulted in a regional-scale spatial landslide susceptibility analysis (LSA) map with five susceptibility classes. Approximately 11.39% (12.99 km^2), 25.56% (29.14 km^2), 29.67% (33.82 km^2), 23.6% (26.9 km^2), and 9.78% (11.15 km^2) are classified as very low, low, moderate, high, and very high susceptibility classes, respectively. Using the area under the curve validation method, the prediction and success rates were 82.63% and 82.6%, respectively. The LSA map is considered reliable because 239 landslides (0.14 km^2) were classified as high to very high susceptibility classes. Therefore, this study provides valuable insights for stakeholders, researchers, and professionals, facilitating the proposal of suitable mitigation measures and the development of robust landslide management plans.

Keywords: Pekan Nabalu; Bundu Tuhan; Kundasang; landslide susceptibility analysis; frequency ration

***Corresponding author**:
Rodeano Roslee
rodeano@ums.edu.my

***Received**: 12 April 2023*
***Revised**: 15 October 2023*
***Accepted**: 16 October 2023*
***Published**: 31 December 2023*

***Citation**:
Roslee, R., and Krishnan, R. B. (2023). Landslide susceptibility assessment in Sabah, Malaysia: A bivariate frequency ratio approach. Science, Engineering and Health Studies, 17, 23020004.

1. INTRODUCTION

Numerous tourists from all around the world visit Pekan Nabalu to Kundasang town to experience its beautiful highland scenery and enjoy the cold weather (Taharin, 2019). The increase in tourism activities (Simon et al., 2014; Tating et al., 2015; Roslee et al., 2017) has led to rapid land use development since 1980 (Komoo and Lim, 2003), Thus development includes slope cutting for road construction and buildings, deforestation, and agricultural activities to promote fresh local crops. For example, several roads near the Tamparuli to Ranau area in Kundasang have been reported to experience creeping land movement following extensive development activities in recent years (Komoo and Lim, 2003; Liew and Gue, 2001; Mohamad et al., 2018; Omar et al., 2020). Moreover, the settlement area has been established within a moderately to highly prone area to landslide events, debris flow and active soil erosion, resulting in mass movements. The accelerated land use development around Kundasang town has also increased the occurrence of mass movements (Figures 1 and 2), affecting infrastructure quality in the region, such as tilted electricity poles, pump

houses, broken drainage systems, and roads (Komoo and Lim, 2003; Mohd Kamal et al., 2019).

The occurrence of landslides around Pekan Nabalu to Kundasang is common due to factors such as active geomorphological processes, geological conditions, and heavy rainfall. Additionally, the presence of active faults induces tremors in the area, leading to mass movements (Tongkul, 2017). Following the 2015 Ranau earthquake, there was an increase in reported cases of landslide reactivation (Wang et al., 2017). However, the severity of the landslide issues in the study area is a result of rapid development in land use planning, a human factor that disturbs the stability of the region and contributes to extensive landslide problems. Hence, there have been numerous reported landslide cases in recent years, causing damages ranging from minimal to major levels. These incidents have resulted in the loss of lives and have affected numerous properties, infrastructures, the economy, and the environment. Due to the impact of landslides around Kundasang, the total loss have amounted to nearly a trillion Malaysian Ringgit (Roslee et al., 2011; Roslee and Jamaludin, 2012; Sharir et al., 2016; Azlan et al., 2017).

Figure 1. Landslide scars can be seen from Jalan Tenompok - Bundu Tuhan, Kundasang, Sabah

Figure 2. Kundasang town that is prone to mass movements and slope failure

The study area is located in the northwest region of Sabah, Malaysia, as depicted in Figure 3. It spans latitudes 5°57′50.02″N to 6°1′57.57″N and longitudes 116°27′19.45″E to 116°35′25.97″E, covering an area of 114 km^2. The region has a hilly terrain with elevation reaching up to 2150 m above sea level, attributed to active tectonism and past geomorphological and geological processes (Mohd Kamal et al., 2019). Notably, the study area is renowned for Mount Kinabalu. Key towns within the study area include Pekan Nabalu, Tenompok, Bundu Tuhan, and Kundasang, connected by major road systems traversing hilly areas and river systems such as Sungai Mesilau. The climate is tropical and characterized by a high rate of rainfall due to the seasonal monsoon.

The rise of the Mount Kinabalu pluton in the past formed major local faults such as Mensaban and Lobou-Lobou, which remain active to this date (Tjia, 2007; Golutin et al., 2022). The strike-slip faults in the study area trend from N–S, NE–SW, and NW–SE, resulting in extensive geological deformation in the past (Tjia, 2007). The study area was uplifted during the Cenozoic era during the Tertiary period, and is underlain by three lithological units. These units begin with the oldest formation, Trusmadi (Paleocene to Eocene age), followed by the Crocker formation (Late Eocene to Early Miocene age), and finally, the deposition of Pinosouk gravel (Pleistocene to Holocene) (Collenette, 1958).

The study area has been identified as highly susceptible to serious landslide events and requiring continuous observation and monitoring. For instance, the Public Works Department (JKR) collaborates actively with several organizations in slope management and rehabilitation along the roads from Bundu Tuhan to Kundasang (Roslee et al., 2018a, 2018b; Roslee, 2019). This study provides valuable insights for stakeholders, professionals, and researchers to develop improved land use planning and landslide management framework, aiming to minimize the negative impacts of landslide occurrences. Therefore, the main objective of this study was to conduct a landslide susceptibility analysis (LSA) of the study area using a quantitative method, specifically the bivariate statistical model, known as the frequency ratio (FR) (Jeong et al., 2018; Norhisham and Roslee, 2019). The FR method assesses the correlation between landslide occurrences in an area and the causative factor, predicting areas prone to future landslide events (Mersha and Meten, 2020). This bivariate method involves integrating a set of weighted independent factors with dependable factors to measure and analyze their statistical relationship (Ehret et al., 2010).

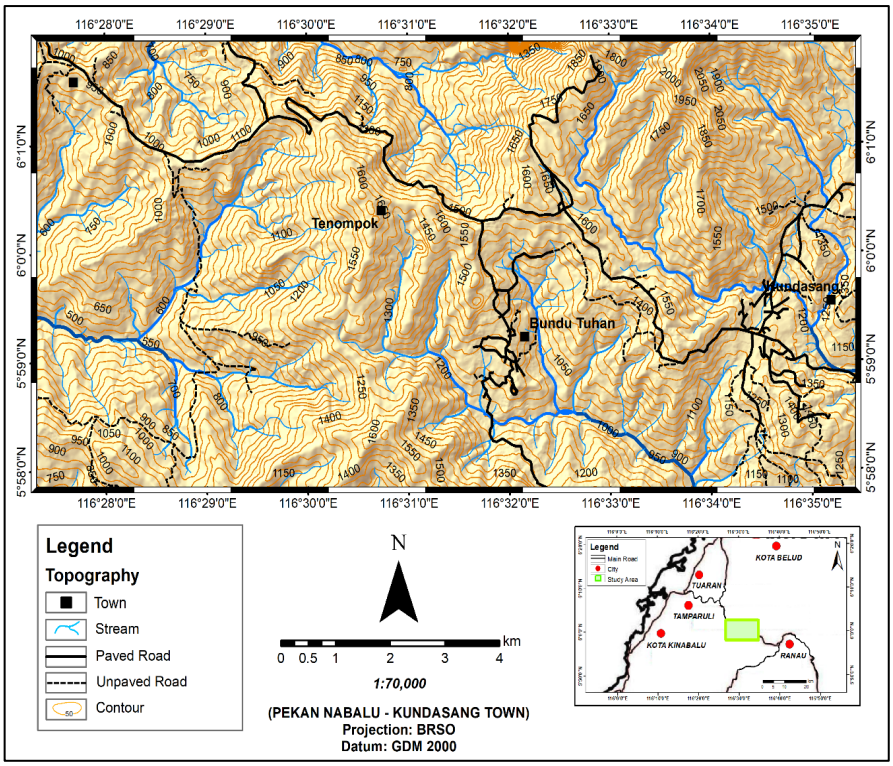

Figure 3. Topography map of the study area

2. MATERIALS AND METHODS

2.1 Landslide inventory database

The methodology of the LSA study consisted of three stages: (1) Compilation of a landslide inventory database; (2) Selection of landslide causative factors, including slope angle, slope aspect, slope curvature, drainage proximity, lineament proximity, land use, soil series, and lithology; (3) Generation of a landslide susceptibility map (LSM) using the bivariate FR model, followed by validation using the area under the curve (AUC) method. The geographic information system software, ArcGIS 10.4, was used as a tool for analysis and map construction in raster format with a pixel size of 1 m × 1 m. The framework of the LSA using bivariate FR analysis is as follows (Figure 4).

2.2 Landslide causative factors

The selected landslide causative factors for this study included slope angle, slope aspect, slope curvature, drainage proximity, lineament proximity, land use, soil series, and lithology. The choice of these factors was grounded in the presence of existing elements that influence slopes stability in the region. This determination was based on the study area's background, the types of landslides and their mechanism, and the causative factors that triggered past landslide occurrences (Guzzetti et al., 1999; Glade and Crozier, 2005; Cao et al., 2021). These causative factors were digitized into thematic map layers for further analysis. For example, the slope angle, slope aspect, and slope curvature thematic layers were derived from the IFSAR digital elevation data (DEM) in ArcGIS 10.4, presented in raster format with a pixel size of 1 m × 1 m. Thematic layers for land use, soil series, and lithology were digitized from polygon vectors, later converted into raster format using secondary data obtained from the Department of Agriculture (DOA) (2018) and the Department of Mineral and Geoscience (2018). Furthermore, the drainage proximity and lineament proximity maps were constructed from DEM and topography maps, respectively. These maps were digitized into line vector layers and subsequently analyzed using the multiple buffer tool in ArcGIS 10.4 to generate proximity thematic maps.

Slope angle

The slope angle, or slope gradient, is an important factor that influences slope stability. It estimates the susceptibility of the slope surface to sliding based on its steepness. The slope angle factor map (Figure 5a) was produced in ArcGIS 10.4 using IFSAR DEM data and the slope tool. This factor was categorized into six classes: flat (<5°), gentle (6°–15°), moderate (16°–25°), steep (26°–35°), very steep (35°–60°), and extremely steep (>60°). The classification follows the geological terrain mapping guidelines (Mohamad and Chow, 2003).

Slope aspect

The slope aspect map shows the direction, grade, and trend of morphology, highlighting areas with potential exposure to landslides (Cellek, 2021). Slope aspect influences slope stability by determining the direction of the exposure to rainfall, sunlight, and wind, consequently affecting erosion (Cellek, 2021). Using ArcGIS 10.4, the slope aspect map (Figure 5b) was derived and analyzed from the IFSAR dataset using the aspect tool. This factor was categorized into eight classes: north, northeast, east, southeast, south, southwest, west, and northwest.

Slope curvature

The slope curvature factor controls the flow of landslide materials down various slope morphologies. It consists of the plan curvature, which determines the curvature geometry of a slope that is perpendicular to the slope direction. This curvature can be either convergent or divergent. Meanwhile, the profile curvature is the curvature geometry of a slope that is parallel to the slope direction, affecting the acceleration of landslide debris (Carson and Kirkby, 1972). For this study, the total curvature factor was considered to consist of convex (negative value), concave (positive value), and flat (zero) surfaces (Mandal and Mandal, 2016). The slope curvature map (Figure 5c) was derived from IFSAR DEM data in ArcGIS 10.4 using the curvature tool and reclassified into three classes: convex, flat, and concave.

Drainage proximity

The stability of a slope is significantly influenced by its proximity to the drainage network. The drainage proximity map was produced based on the basis of the drainage map derived from the IFSAR DEM data. The resulting drainage map (Figure 5d) was analyzed using multiple buffer rings to create a proximity map classified into five classes with a 200-m interval: <200, 200–400, 400–600, 600–800, 800–100, and >1000 m.

Lineament proximity

Lineaments indicate underlying structural features, such as faults or joint fractures, displaying linear lines on the topography's surface (Murasingh and Jha, 2013; Prabu and Rajagopalan, 2013). These features may exhibit displacement near fault zones, significantly impacting the slope stability of the area. Using satellite images and IFSAR data, the lineaments reveal the direction of regional deformation due to past tectonism. Positive lineaments represent ridges and ranges, while negative lineaments represent rivers and valleys (Ahmadi et al., 2023). The lineament proximity map was produced based on a combined positive and negative lineament vector layer derived from the satellite imagery and drainage map. The resulting lineament map (Figure 5e) was analyzed using multiple buffer rings to produce a proximity map classified into five classes with a 200-m interval: <100, 101–200, 201–300, 301–400, 401–500, and >500 m.

Land use

Land use describes the development and management of land in an area. Base on the land use map, it is possible to analyze potential areas exposed to landslide susceptibility (Roccati et al., 2021). The land use map was obtained from the DOA and revised using recent satellite imagery from Google Earth in 2021. The land use factor map (Figure 5f) was digitized and analyzed in ArcGIS 10.4 using polygons in the Editor tool, based on the provided land use map. Subsequently, the land use factor map was classified into several classes: barren land, built-up, cultivation, and forest.

Soil series

The soil series factor describes the properties and characteristics of the soil in the study area. The strength of soil and weathered rock materials produced by different parent materials has a major influence on slope stability (Komadja et al., 2021). The soil series map was obtained from the DOA. Using ArcGIS 10.4, the soil series map (Figure 5g) was digitized using polygons in the Editor tool based on the obtained soil series map. The soil series map was classified into three classes: Crocker, Trusmadi, and Pinosouk soils (British Government's Overseas Development Administration (Land Resources Division), 1974).

The Crocker and Trusmadi soil series consist of parent material composed of sandstone and mudstone, originating from mountain landforms. In the Crocker series, the primary soil units include Orthic Acrisols, Lithosol, and Chromic and Dystric Cambisols. Conversely, the Trusmadi series is characterized by Gleyic and Orthic Acrisols, Gleyic Podzol, Humic Gleysols, Dystric Histosols, and Lithosol as its major soil units. The Pinosouk soil series, originating from a plateau with a horizontally undulating surface and dissected terraces with slopes above 25, is composed of colluvium, sandstone, and mudstone. Its major soil units include Gleyic Podzol, Gleyic and Orthic Acrisols, and Humic and Dystric Gleysols.

Lithology

The lithology map shows the distribution of lithological units in an area, consisting of rock units and geological formations that influence slope stability. The physical characteristics of each lithology, such as texture, composition, and grain size, affect the weathering rate, strength of rock and soil material, as well as porosity, and permeability. The lithology map was obtained from the Department of Mineral and Geoscience. Using ArcGIS 10.4, the lithology factor map (Figure 5h) was digitized using polygons in the Editor tool based on the obtained geological map. The lithology map is classified into three classes: (i) Crocker, (ii) Trusmadi, and (iii) Pinosouk gravel.

The lithology of the Trusmadi formation consists of strongly faulted and shear metasedimentary rocks that have undergone low-grade metamorphism, including argillaceous rocks, phyllite, thick shale interbedded with thin sandstone, slate, massive sandstone interbedded with siltstone, and mudstone trending in orientations NW–SE and NE–SW (Collenette, 1958; Tongkul, 2007). The

Crocker formation represents turbidite deposition with lithological units like massive sandstone interbedded with shale, red and gray shale, siltstone, and mudstone, also trending from orientations NW–SE and NE–SW (Collenette, 1958; Tongkul, 2007). The youngest rock unit, Pinosouk gravel deposition, is composed of poorly consolidated tilloid deposits with blocks of gravels and granodiorite boulders mixed with a mud matrix (Collenette, 1958).

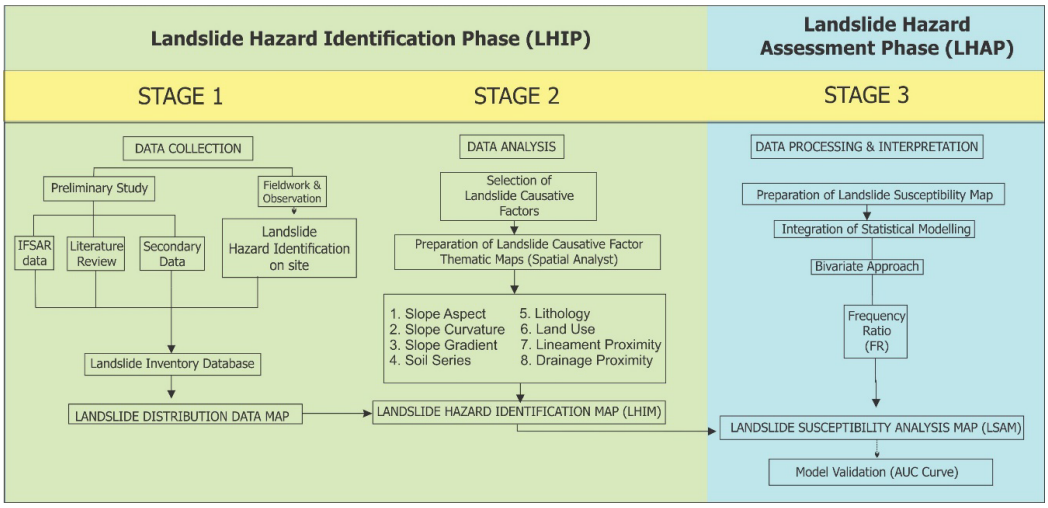

Figure 4. Framework of LSA using bivariate FR model

2.3 Landslide susceptibility assessment using the FR

The bivariate FR model was selected to assess the probability of landslide occurrences within the study area by examining the correlation between the landslide distribution and landslide causative factors. This model evaluates the ratio of the landslide area in individual landslide causative factor classes to the total study area. The expression of the FR is shown in Equation (1) (Lee and Talib, 2005).

$$FR = \frac{\left(\frac{Mi}{M}\right)}{\left(\frac{Ni}{N}\right)} \quad (1)$$

where *FR* is the frequency ratio, *Mi* is the area of landslides in the subclass of each landslide causative factor, *M* is the total area of landslides in the study area, *Ni* is the area of subclass of each landslide causative factor in the study area, and *N* is the total study area.

All landslide causative factor layers (independent factor) and landslide distribution layers (dependent factor) were intersected in ArcGIS 10.4 using the tabulate area tool to obtain the number of landslide pixels within each subclass of a factor. These data were tabulated in Microsoft Excel (Table 1) to calculate the FR values. To produce an LSM, the obtained FR values were multiplied by their respective rasterized factor map layers. Finally, the landslide susceptibility index (LSI) values (Equation (2)) were obtained when the factor maps were summed using the Raster Calculator in ArcGIS 10.4 (Lee and Talib, 2005).

$$LSI = \sum_{i=1}^{n} FR_i X_i \quad (2)$$

where *n* is the total number of landslide causative factors, FR_i is the FR of each landslide causative factor, and *Xi* is the individual landslide causative factors.

The LSI values were further grouped into five landslide susceptibility classes, namely, very low, low, moderate, high, and very high, using Natural Break. Accordingly, the areas with a high probability of landslide occurrence exhibit an FR value >1, whereas the areas with a low probability of landslide occurrence have an FR value <1.

2.4 Model validation

The validation of the model involves the integration of the landslide inventory map and LSM. Initially, the landslide inventory database was divided randomly in ArcGIS 10.4 to reduce bias. Of the landslides, 70% and 30% were selected for the training and testing datasets, respectively. The training and testing datasets were used to produce the success and prediction rate values, respectively. The AUC of the success rate was used to test the reliability of the model in classifying landslide occurrences in the generated LSM area, whereas the AUC of the prediction rate showed the ability of the model to predict the accuracy of the landslide susceptibility zones. The model with the highest success rate provides insights into the possibility of future landslides occurring in an area similar to that of existing landslides, and the model with the highest prediction accuracy signifies the highest validation accuracy.

To calculate the success and prediction rates, the methodology proposed by Chung and Fabbri (1999) was followed. The LSM was subjected to reclassification into 100 classes using the Natural Break tool. The reclassified LSM was intersected with both training and testing landslide datasets to derive integrated index values. Next, the obtained index values were analyzed using Microsoft Excel to calculate a cumulative landslide percentage value. Finally, these index values were plotted into a line graph where the X- and Y-axes represent the reclassified landslide susceptibility classes up to 100 classes and cumulative landslide percentage for the entire study area, respectively. If the slope of the curves is closer to the Y-axis, it indicates a high rate of landslide occurrences in the landslide susceptibility class.

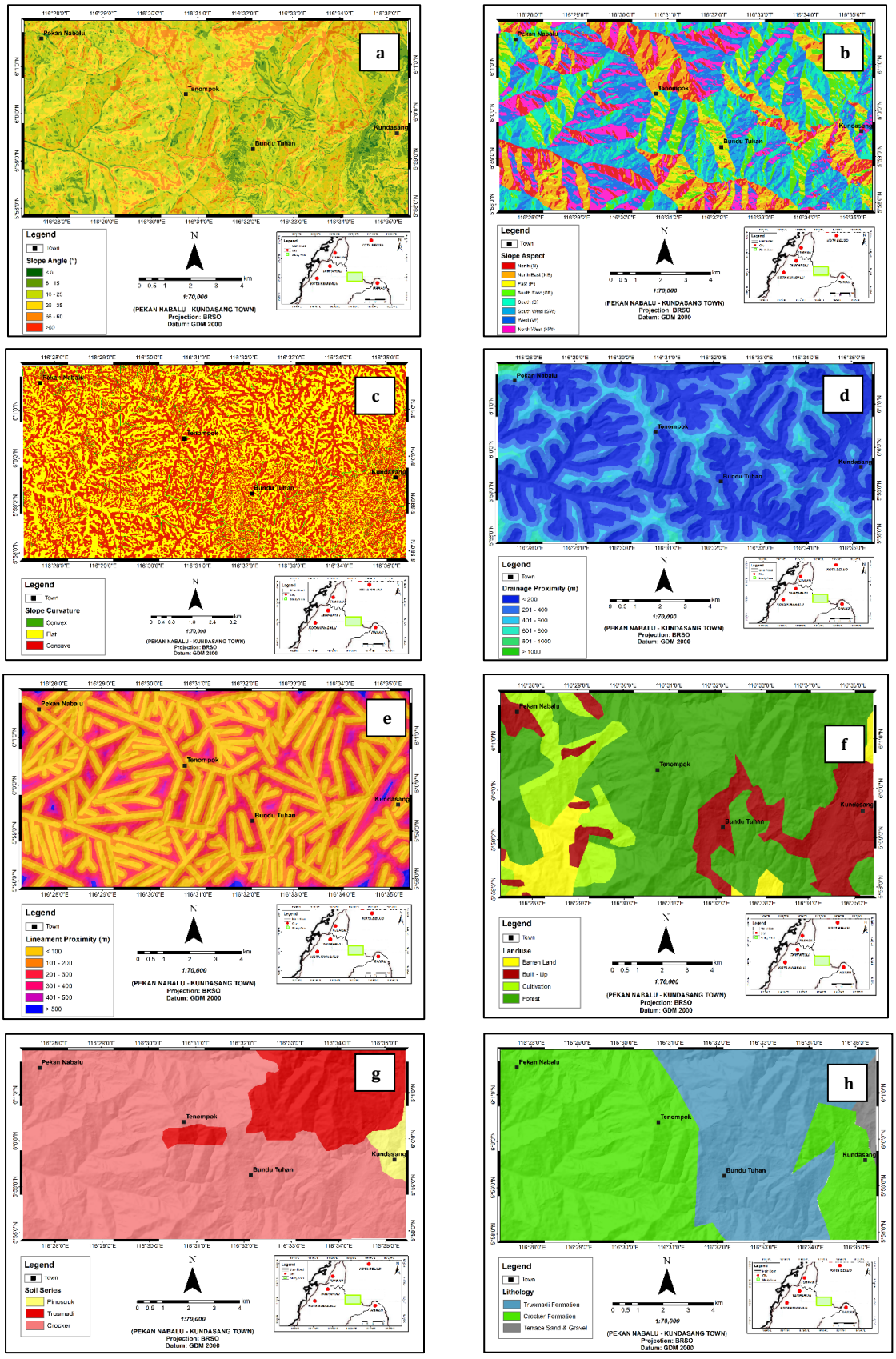

Figure 5. Landslide causative factor thematic maps: (a.) slope angle, (b.) slope aspect, (c.) slope Curvature, (d.) drainage proximity, (e.) lineament proximity, (f.) land use, (g.) soil series, and (h.) lithology

3. RESULTS AND DISCUSSION

To assess the susceptibility of the study area to landslide events using the FR model, a total of eight landslide causative factors—namely, slope angle, slope curvature, slope aspect, drainage proximity, lineament proximity, soil series, land use, and lithology—were selected for integration with the landslide distribution map. Based on the landslide distribution map produced from the Google Earth satellite image, IFSAR dataset, and field observations, a total of 564 (covering 0.27 km^2) landslides were identified and digitized into a landslide distribution map. Out of these landslides, 70% (396 landslides, covering 0.19 km^2) were randomly selected as the training landslide dataset to generate the model, while the remaining 80% (168 landslides, covering 0.08 km^2) were selected as the testing dataset for validation purposes. The landslide causative factors and their computed FR values are shown in Table 1.

Table 1. Relationship between landslide causative factors and landslide distribution using FR

Factor/Classes	Total landslide	Landslide area percentage (A)	Total subclass pixels in factors	Subclass Pixels (B)	Frequency Ratio (A/B)
Slop angle					
0–5	1954	0.72	1145788	1.01	0.71
6–15	27923	10.23	14144754	12.44	0.82
16–25	108791	39.84	42879171	37.69	1.06
26–35	89647	32.83	43828775	38.52	0.85
36–60	44742	16.39	11756404	10.34	**1.59**
>60	0	0.00	5541	0.00	0.00
Slope aspect					
North (0–22.5), (337.5 - 360)	27263	9.98	11039635	9.70	1.03
Northeast (22.5–67.5)	26498	9.70	12494718	10.98	0.88
East (67.5–112.5)	27462	10.06	11167671	9.82	1.02
Southeast (112.5–157.5)	38036	13.93	13783765	12.12	1.15
South (157.5–202.5)	52114	19.09	16156634	14.20	**1.34**
Southwest (202.5–247.5)	50742	18.58	18725589	16.46	1.13
West (247.5–292.5)	24784	9.08	17274325	15.18	0.60
Northwest (292.5–337.5)	26159	9.58	13117995	11.53	0.83
Slope curvature					
Convex	10862	3.98	2417241	2.12	**1.87**
Flat	146937	53.81	54440644	47.85	1.12
Concave	115257	42.21	56902447	50.02	0.84
Drainage proximity					
>200	167264	61.26	57990491	50.96	**1.20**
201–400	81442	29.83	39527334	34.94	0.85
401–600	23786	8.71	14601878	12.67	0.69
601–800	509	0.19	1319158	1.14	0.16
801–1000	55	0.02	230356	0.20	0.10
>1000	0	0.00	91115	0.08	0.00
Lineament proximity					
<100	125052	45.80	46929510	41.37	1.11
101–200	90161	33.02	37549576	33.23	0.99
201–300	40965	15.00	19007220	16.49	0.91
301–400	13282	4.86	7000013	6.07	0.80
401–500	2671	0.98	2439104	2.12	0.46
>500	925	0.34	834910	0.72	0.47
Lithology					
Pinosouk Gravel	3888	1.42	2169117	1.89	0.75
Crocker Formation	141433	51.80	6862411	60.32	0.86
Trusmadi Formation	127735	46.78	42968804	37.79	**1.24**
Soil series					
Crocker	224321	82.15	89270749	78.49	1.05
Trusmadi	40079	14.68	20337944	19.44	0.76
Pinosouk	8656	3.17	4151638	2.07	**1.53**
Land use					
Barren Land	11492	4.21	7284693	6.40	0.66
Built-Up	67076	24.57	20870557	18.35	**1.34**
Cultivation	28325	10.37	12540175	11.02	0.94
Forest	166163	60.85	73064907	64.23	0.95

The slope angles of 36°–60° and 16°–25° exhibited high FR values at 1.59 and 1.06, respectively. Landslides are more common on steeper slopes due to gravitational pull on the slope surface, reducing its stability. The decrease in the shear strength of the surface causes the landslide material to move easily against the frictional force compared to gentle slopes with nearly horizontal surfaces (Highland and Bobrowsky, 2008). The slope aspect facing south, southeast, southwest, north, and east orientations showed high FR values at 1.34, 1.15, 1.13, 1.03, and 1.02, respectively, indicating a high correlation with landslide occurrences. Similar slope aspects—southwest, east, south, north, and southeast—were found to contain high landslide density in a landslide study around the Kundasang area (Sharir et al., 2017). The south-facing slope, with the highest FR value, receives more sun exposure, moisture, and rainfall during the monsoon season, with lower vegetation coverage compared to other orientation. Landslide distribution was also higher in convex slopes and flat surfaces with high FR values at 1.87 and 1.12, respectively. Convex slopes are the most prone to slope failure compared with flat and concave surfaces due to their upward convex geometry, which can hold water for extended period (Lee and Talib, 2005), leading to saturation and rapid erosion, resulting in slope failure.

The proximity to drainage below 200 m had the highest FR value at 1.20, indicating a strong correlation with landslide events. Slopes near drainage system often have lower stability due to the potential for a high groundwater table, facilitating water infiltration into the slope. Additionally, the areas with steep hillslopes and valleys sides are susceptible to erosion from fast-flowing river water (Akgun and Turk, 2011), driven by heavy rainfall or a rapid increase in groundwater discharge into the river. The proximity to the lineament below 100 m also has the highest landslide distribution, with a high FR value of 1.11. The susceptibility to landslide occurrences increases when the slopes are closer to the lineament features. Features such as faults, folds, or shear zones are weak due to deformation from weathering and past tectonic processes. Consequently, slopes in this zone are more prone to landslides, especially triggered by factors such as rainfall or earthquakes (Kanungo et al., 2009).

The Trusmadi formation lithology showed the highest FR value at 1.24, indicating a positive correlation with landslide occurrences. The lithological units of this formation are metamorphosed metasedimentary rock units, consisting of angular to subangular argillaceous rocks, phyllite, mudstone, and slate. These materials are highly susceptible to active mechanical and chemical weathering. As a result, the production of clay minerals weakens soil strength, leading to soil erosion and slope instability. Furthermore, the high presence of extreme faulting and sheared zones in the Trusmadi formation makes it susceptible to landslide occurrences; therefore, landslides in this formation would occur easily.

However, the landslide distribution for the soil series classes Pinosouk and Crocker had a greater landslide distribution with FR values of 1.53 and 1.05, respectively. These soil series are composed of colluvium materials, weathered sandstone, and mudstone. Colluvium soil is a loose unconsolidated, heterogeneous mass of earth material deposited at the base of a slope, consisting of degraded soil and rock fragments of various minerals, shapes, and sizes (Turner and Jayaprakash, 1996). This type of soil resulted from active weathering and erosion, as it is rich in clay minerals. The high expansion and shrinkage rate of the fine clay mineral in the presence of water weakens the slope strength, leading to slope failure (Jiang et al., 2013).

Built-up land use had the highest FR value of 1.34. Excessive land use planning resulted in less vegetation coverage and further degraded the soil strength and quality over time, reducing slopes stability in the area. Bundu Tuhan, Kampung Dumpiring, and Kundasang town experience high mass movements and landslides as more land is developed for tourism and agricultural purposes. Additionally, overloaded slopes with poor monitoring and no structural maintenance can experience slope failure easily.

Finally, the LSM (Figure 6) produced using the FR model is classified into five susceptibility classes: very low (12,962,018 pixels), low (29,078,971 pixels), moderate (33,748,955 pixels), high (26,845,192 pixels), and very high (11,125,196 pixels). On the basis of the landslide susceptibility classification index results (Figure 6), 11.39% (12.99 km^2) of the study area is classified as very low susceptibility class, followed by 25.56% (29.14 km^2), 33.82% (29.67 km^2), 23.6% (26.9 km^2), and 9.78% (11.15 km^2) for low, moderate, high, and very high susceptibility classes, respectively.

The landslide distribution map was integrated with the LSM of the study area (Table 2 and Figure 7). In the very low susceptibility class (14,514 pixels), 48 landslides (5.315%, covering 0.015 km^2) were located, while in the low susceptibility class (39,257 pixels), 111 landslides (14.38%, covering 0.039 km^2). The moderate susceptibility class (75,660 pixels) contained 166 landslides (27.71%, covering 0.076 km^2), the high susceptibility class (88,884 pixels) had 164 landslides (32.55%, covering 0.089 km^2), and the very high susceptibility class (54,741 pixels) had 75 landslides (20.05%, covering 0.055 km^2).

In general, areas classified as very low and low landslide susceptibility classes have minimal landslide activity because the slopes are stable and situated on low-lying terrain. On the other hand, moderate, high and very high landslide susceptibility classes have high landslide activity due to greater potential for slope instability as these areas have steeper slope and are situated at higher elevations.

Based on Figure 8, there are 159 landslides in the very low to low landslide susceptibility classes, indicating that this region requires minimal observation and monitoring due to greater slope stability. However, the total number of landslides in the moderate susceptibility classes is 166, requiring frequent monitoring and observation of potential areas prone to slope failures. The high and very high landslide susceptibility classes comprise the highest landslide distribution, totalling 239 landslides. These classes consist of very unstable areas and risky slopes. To ensure the safety of the nearby localities and communities from the impacts of the landslide hazard, development activities and any land use planning should be prohibited around this region and immediate slope management mitigation should be conducted.

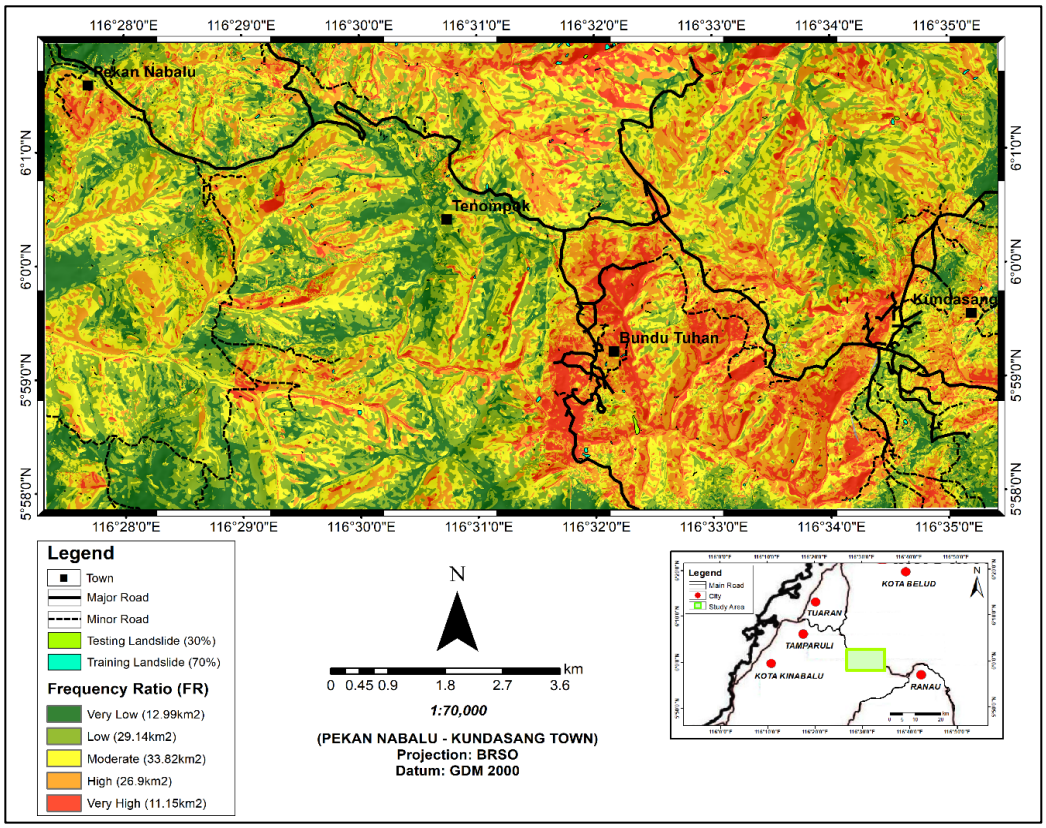

Figure 6. The LSM produced using the FR model

Table 2. Relationship between the landslide distribution and the landslide susceptibility classes

Susceptibility class	No. of class pixels	Area of class (km²)	Percentage of area covered (%)	Number of landslides	No. of landslide pixels	Area of landslide (km²)	Percentage of area landslide covered
Very Low	12962018	12.99	11.390	48	14514	0.015	5.315
Low	29078971	29.14	25.560	111	39257	0.039	14.377
Moderate	33748955	33.82	29.670	166	75660	0.076	27.709
High	26845192	29.90	23.600	164	88884	0.089	32.552
Very High	11125196	11.15	9.780	75	54741	0.055	20.048

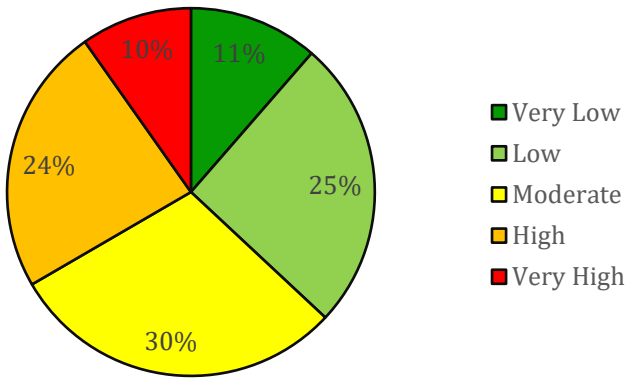

Figure 7. Comparison of the percentage of landslide susceptibility classes of the FR model

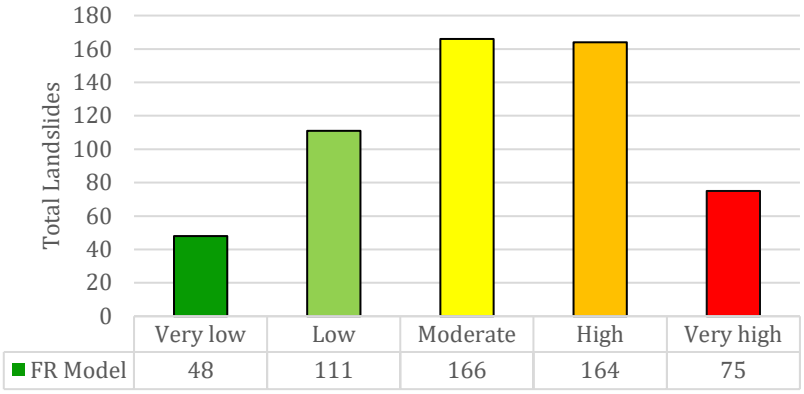

Figure 8. Landslides in different susceptibility classes of the FR model

Based on the validation of the FR model (Figure 9) using the training (70% landslides) and testing (30% landslides) datasets, the AUC showed a success rate curve of 82.6%, and the prediction rate curve was 82.63%. AUC above 80% indicated that the LSM produced using the FR model is accurate and reliable. Moreover, the slopes of both the success and prediction rate curves were observed leaning closer toward the Y-axis and were steep, indicating a high correlation of the landslide distribution to the susceptibility classes of landslide occurrences, hence, a higher probability of landslide occurrences in the study area.

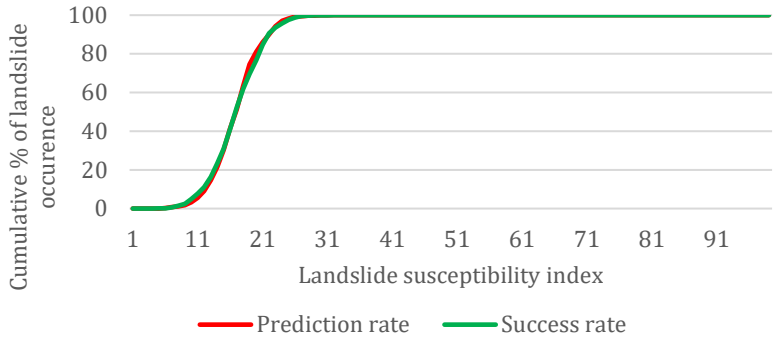

Figure 9. Validation of the frequency ratio (FR) model using AUC curve

4. CONCLUSIONS

Considering the available information, the following conclusions may be drawn from this study: A total of eight landslide causative factors were selected: slope angle, slope aspect, slope curvature, soil series, lithology, land use, drainage proximity, and lineament proximity. Using Google Earth satellite images, the IFSAR dataset, and field observations, approximately 564 landslides (covering 0.27 km^2) were identified and digitized into a landslide distribution map. Of the landslides, 70% (396 landslides, covering 0.19 km^2) were selected as the training landslide dataset to produce the success rate curve, while the remaining 30% landslides (168 landslides, covering 0.08 km^2) were selected as the testing dataset to produce the prediction rate curve. To produce the LSM, the landslide causative factor maps (independent factors) were integrated with the landslide distribution map (dependent factors) of the area. As a result, approximately 11.39% (12.99 km^2), 25.56% (29.14 km^2), 29.67% (33.82 km^2), 23.6% (26.9 km^2), and 9.78% (11.15 km^2) were classified as very low, low, moderate, high, and very high susceptibility classes, respectively. The generated LSM was validated using the AUC. From the analysis, the success and prediction rates of the model were 82.6% and 82.63%, respectively. Approximately 239 landslides (covering 0.14 km^2), which is 52.6% of the total landslides, were classified as high to very high susceptibility classes. Based on the FR values, subclasses contributing to landslide occurrences in the study area are slope angle between 35° and 60°, convex slopes, slope aspect in south orientation, built-up land use type, Crocker soil series, Trusmadi formation lithology, drainage proximity under 200 m, and lineament proximity under 100 m.

A wide range of the study area is highly susceptible to landslides; therefore, a thorough landslide management plan is suggested to be conducted by experts and relevant stakeholders.

REFERENCES

Ahmadi, H., Pekkan, E., and Seyitoğlu, G. (2023). Automatic lineaments detection using radar and optical data with

an emphasis on geologic and tectonic implications: A case study of Kabul Block, eastern Afghanistan. *Geocarto International*, 38 (1), 2231400.

Akgun, A., and Turk, N. (2011). Mapping erosion susceptibility by multivariate statistical method: A case study from the Ayvalik region. *Computers & Geosciences*, 37(9), 1515–1524.

Azlan, N. N. N, Simon, N., Hussein, A., Roslee, R., and Ern, L. K. (2017). Chemical properties characterization of failed slopes along the Ranau-Tambunan road, Sabah, Malaysia. *Sains Malaysiana*, 46(6), 867–877.

British Government's Overseas Development Administration. (1974) The soils of sabah: Soils sheet NB 50-10 (Kota Kinabalu). The Ordance Survey. [Online URL: https://esdac.jrc.ec.europa.eu/images/Eudasm/Asia/images/maps/download/MY3007_5SO.jpg] accessed on May 12, 2023.

Cao, Y., Wei, X., Fan, W., Nan, Y., Xiong, W., and Zhang, S. (2021). Landslide susceptibility assessment using the weight of evidence method: A case study in Xunyang area China. *PLoS ONE*, 16(1), 20245668.

Carson, M. A., and Kirkby, M. J. (1972). *Hillslope Form and Process*. London: Cambridge University Press.

Cellek, S. (2021). The effect of aspect on landslide and its relationship with other parameters. In *Landslides* (Zhang, Y., and Cheng, Q., Eds.), pp. 1–19. IntechOpen.

Chung, C. J. F., and Fabbri, A. (1999). Probabilistic prediction models for landslide hazard mapping. *Photogrammetric Engineering and Remote Sensing*, 65(12), 1389–1399.

Collenette, P. (1958). The geology and mineral resources of Jesselton – Kinabalu area, North Borneo. In *British Territories in Borneo. Geological Survey Department. Memoir No.6,* pp. 1–194. Kota Kinabalu: Geological Survey Department.

Ehret, D., Rohn, J., Dumperth, C., Eckstein, S., Ernstberger, S., Otte, K., Rudolph, R., and Wiedenmann, J. (2010). Frequency ratio analysis of mass movements in the Xiangxi catchment, three gorges reservoir area, China. *Journal of Earth Science*, 21(6), 824–834.

Glade, T., and Crozier, M. J. (2005). The nature of landslide hazard impact. In *Landslide Hazard and Risk* (Glade, T., Anderson, M. and Crozier, M., Eds.), pp. 3–74. [Online URL: https://onlinelibrary.wiley.com/doi/abs/10.1002/9780470012659.ch2] accessed on May 2, 2023.

Golutin, B., Tongkul, F., and Rahim, I. A. (2022). Intraplate crustal deformation in Sabah: Preliminary results of Global Positioning System/Global Navigation Satellite System measurements in the Ranau area. *Bulletin of the Geological Society of Malaysia*, 74(1), 111–122.

Guzzetti, F., Carrara, A., Cardinali, M., and Reichenbach, P. (1999). Landslide hazard evaluation: A review of current techniques and their application in a multi-scale study, Central Italy. *Geomorphology*, 31(1–4), 181–216.

Highland, L. M., and Bobrowsky, P. (2008). The landslide handbook – a guide to understanding landslides. In *Circular 1325*, p. 129. Virginia: US Geological Survey.

Jeong, S., Kassim, A., Hong, M., and Saadatkhah, N. (2018). Susceptibility assessments of landslides in Hulu Kelang area using a geographic information system – Based prediction model. *Sustainability*, 10(8), 2941.

Jiang, H., Wang, B., Inyang, H. I., Liu, J. Gu, K., and Shi, B. (2013). Role of expansive soil and topography on slope failure and its countermeasures, Yun County China. *Engineering Geology*, 152, 155–161.

Kanungo, D. P., Arora, M. K., Sarkar, S., and Gupta, R. P. (2009). Landslide susceptibility zonation (LSZ) mapping—a review. *Journal of South Asia Disaster Study*, 2(1), 81–105.

Komadja, G. C., Pradhan, S. P., Oluwasegun, A. D., Roul, A. R., Stanislas, T. T., Laïbi, R. A., Adebayo, B., and Onwualu, A. P. (2021). Geotechnical and geological investigation of slope stability of a section of road cut debris-slopes along NH-7, Uttarakhand, India. *Results in Engineering*. 10, 100227.

Komoo, I., and Lim, C. S. (2003). The Kandasang landslide complex: A detailed mapping of the Kandasang National Secondary School area. *Bulleting of the Geological Society of Malaysia*, 46, 387–392. [in Malaysian]

Lee, S., and Talib, J. A. (2005). Probabilistic landslide susceptibility and factor effect analysis. *Environmental Geology*, 47, 982–990.

Liew, S. S., and Gue, S. S. (2001) Massive creep movements of post-glacial deposits in Kundasang areas. In *GSM-IEM Forum: Engineering Geology and Geotechnical Slopes*, p. 13. Kuala Lumpur, Malaysia: Gua & Partners Sdn. Bhd.

Mandal, B., and Mandal, S. (2016). Assessment of mountain slope instability in the Lish River basin of Eastern Darjeeling Himalaya using frequency ratio model (FRM). *Modeling Earth Systems and Environment*, 2, 121.

Mersha, T., and Meten, M. (2020). GIS-based landslide susceptibility mapping and assessment using bivariate statistical methods in Simada area, northwestern Ethiopia. *Geoenvironmental Disasters*, 7, 20.

Mohamad, Z., and Chow, W. S. (2003). Geological terrain mapping in Cameron Highlands district, Pahang. *Bulletin of the Geological Society of Malaysia*, 46, 69–73. [in Malaysian]

Mohamad, Z., Ramli, Z., Abd Rahman, M. Z., Mohd Salleh, M. R., Ismail, Z., and Abdul Khanan, M. F. (2018). Vulnerability mapping and analysis: An implementation in Geohazard areas in Sabah. *The International Archives of the Photogrammetry, Remote Sensing and Spatial Information Sciences*, 42, 189–200.

Mohd Kamal, N. A., Razak, K. A., and Rambat, S. (2019). Land use/land cover assessment in a seismically active region in Kundasang, Sabah. *The International Archives of the Photogrammetry, Remote Sensing and Spatial Information Sciences*, 42, 433–440.

Murasingh, S., and Jha, R. (2013). Identification of groundwater potential zones using remote sensing and GIS in a mine area of Odisha. In *National Conference: Approaches to Water Resource Management*, Dhanbad, Jharkhand. December 9–10.

Norhisham, M. N., and Roslee, R. (2019). Geohazard assessment in the Kota Kinabalu area, Sabah, Malaysia. *Journal of Physics: Conference Series*, 1358(1), 012068.

Omar, S., Mohamed, Z., and Jais, I. B. M. (2020). Evaluation of the Kundasang ground movement based on geological, geotechnical investigations and stability modelling. *Journal of Physics: Conference Series*, 1529(2), 022036.

Prabu, P., and Rajagopalan, B. (2013). Mapping of Lineaments for Groundwater Targeting and Sustainable Water Resource Management in Hard Rock Hydrogeological Environment Using RS-GIS. In *Climate Change and Regional/Local Responses.* pp. 235–247. London, UK: InTech.

Roccati, A., Paliaga, G., Luino, F., Faccini, F., and Turconi, L. (2021). GIS-based landslide susceptibility mapping for land use planning and risk assessment. *Land*, 10(2), 162.

Roslee, R. (2019). Landslide Risk Management (LRM): Towards a Better Disaster Risk Reduction (DRR) Programme in Malaysia. *ASM Science Journal*, 12(3), 70–81.

Roslee, R. and Jamaludin, T.A. (2012). Landslide hazard vulnerability (LHV): Literature review and proposed new approaches for landslide risk management in Malaysia. *Bulletin of the Geological Society Malaysia*, 58, 75–88. [in Malaysian]

Roslee, R., Felix T., and Norbert S. (2018a). A comparative evaluation of normal polygon geotechnical deterministic analysis (NPGDA) and GEOStatistical INterpolation Techniques (Kriging) (GEOSTAINT-K): A case study from Kota Kinabalu area, Sabah, Malaysia. *ASM Science Journal*, 11(2), 1–18.

Roslee, R., Felix T., Termizi, A. K., and Norbert S. (2018b). Application of analytical hierarchy process (AHP) and factor analysis model (FAM) for landslide susceptibility analysis (LSA) at Kota Kinabalu area, Sabah, Malaysia. *ASM Science Journal*, 11(3), 18–30.

Roslee, R., Jamaludin, T. A., and Simon, N. (2017). Landslide vulnerability assessment (LVAs): A case study from Kota Kinabalu, Sabah, Malaysia. *Indonesian Journal on Geoscience*, 4(1), 49–59.

Roslee, R., Jamaludin, T. A., and Talip, M. A. (2011). GIS applications in landslide risk assessment (LRA): A case study from the Kota Kinabalu city surrounding area, Sabah, Malaysia. *Bulletin of the Geological Society Malaysia*, 57, 69–83. [in Malaysian]

Sharir, K., and Roslee, R. (2022). Flood susceptibility assessment (FSA) using GIS-based frequency ratio (FR) model in Kota Belud, Sabah, Malaysia. *International Journal of Design & Nature and Ecodynamics*, 17(2), 203–208.

Sharir, K., Roslee, R., Ern, L. K., and Simon, N. (2017). Landslide factors and susceptibility mapping on natural and artificial slopes in Kundasang, Sabah. *Sains Malaysiana*, 46(9), 1531–1540.

Sharir, K., Simon, N., and Roslee, R. (2016). Regional Assessment on the influence of land use related factor on landslide occurencces in Kundasang, Sabah. *AIP Conference Proceedings*, 1784, 060015.

Simon, N., Roslee, R., Marto, N. L, Akhir, J. M., Rafek, A. G. and Lai, G. T. (2014). Lineaments and their association with landslide occurences along the Ranau-Tambunan road, Sabah. *Electronic Journal for Geotechnical Engineering*. 19, 645–656.

Taharin, M. R. (2019). Ordinary Kriging as a method to determine the clay mapping distribution in highland area of Sabah. *International Journal of Integrated Engineering*. 11(8), 268–278.

Tating, F. F., Hack, R., and Jetten, V. (2015). Landslide susceptibility assessment using information value statistical method: A case study on Northern Kota Kinabalu, Sabah. *Malaysian Journal of Remote Sensing & GIS*, 4(2), 92–109.

Tjia, H. D. (2007). Kundasang (Sabah) at the intersection of regional fault zones of quaternary age. *Bulletin of the Geological Society of Malaysia*, 53, 59–66. [in Malaysian]

Tongkul, F. (2007). Geological inputs in road design & construction in mountainous areas of West Sabah, Malaysia. In *Proceedings of the 2nd Malaysia – Japan Symposium on Geohazards & Geoenvironmental Engineering, Bangi*, pp. 39–43. Bayview Hotel, Langkawi.

Tongkul, F. (2017). Active tectonics in Sabah—seismicity and active faults. *Bulletin of the Geological Society Malaysia*, 64, 27–36. [in Malaysian]

Turner, A. K., and Jayaprakash, G. P. (1996). Landslides: Investigation and mitigation. In *Transportation Research Board*, p. 685. National Academy of Sciences. [Online URL: chrome-extension://efaidnbmnnnibpcajpcglclefindmkaj/https://onlinepubs.trb.org/Onlinepubs/sr/sr247/sr247-001.pdf] accessed on May 12, 2023.

Wang, Y., Wei, S., Wang, X., Lindsey, E. O., Tongkul, F., Tapponnier, P., Bradley, K., Chan, C. H., Hill, E. M., and Sieh, K. (2017). The 2015 Mw 6.0 Mt. Kinabalu earthquake: An infrequent fault rupture within the Crocker fault system of East Malaysia. *Geoscience Letter*, 4(6), 1–12.